Article

Single-Atom Co−N$_4$ Sites Mediate C=N Formation via Reductive Coupling of Nitroarenes with Alcohols

Xixi Liu,[||] Liang Huang,[||] Yurong He,[||] Peng Zhou, Xuedan Song, and Zehui Zhang*

Cite This: *JACS Au* 2024, 4, 3436−3450

Read Online

ACCESS | 📊 Metrics & More | 📖 Article Recommendations | 🆂🅸 Supporting Information

ABSTRACT: It remains challenging to construct C=N bonds due to their facile hydrogenation. Herein, a single Co atom catalyst was discovered to be active for the selective construction of C=N bonds toward the synthesis of imines and *N*-heterocycles via reductive coupling of nitroarenes with various alcohols, including inert aliphatic ones. DFT calculations and experimental data revealed that the transfer hydrogenation proceeded via the intramolecular hydride transfer and the transfer of H from the α-C$_{sp3}$-H bond to the nitro group was the rate-determining step. The single Co atoms served as a bridge to transfer the electrons from the catalyst to the adsorbed alcohol molecules, resulting in the activation of the α-C$_{sp3}$-H bond. Unlike metal nanoparticles, the C=N bonds in imine products can be reserved due to the large steric hindrance from substituents on C and N. DFT calculation also confirmed that transfer hydrogenation of the C=N bonds in imines is thermodynamically unfavored with a much higher energy barrier compared with the transfer hydrogenation of the −NO$_2$ group (1.47 vs 1.15 eV).

Intramolecular hydride transfer

Advantages
● High activity at base-free conditions
● High selectivity for C=N bond construction
● Wide substrate scope including inert aliphatic alcohols

KEYWORDS: reductive coupling reaction, C5N bonds, nitro compounds, biomass-derived alcohols, single Co atom catalyst
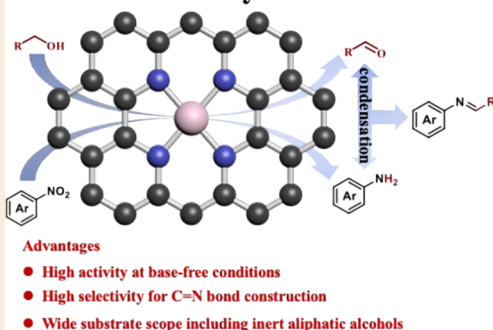
INTRODUCTION

Nitrogen-containing chemicals have been extensively used in many fields, such as fine chemicals, pharmaceuticals, and molecular motors.[1] Therefore, great effort has been devoted to synthesizing different kinds of nitrogen-containing chemicals, such as amines, imines, and *N*-heterocycles, and the key to access these value-added chemicals was the construction of C=N bonds.[2,3] Traditionally, C=N bonds were formed by the acid-catalyzed condensation of carbonyl groups and amines or ammonia, which were limited to the active carbonyl compounds and encountered difficulty in the disposal of acid wastes.[2] Therefore, great effort has been devoted to the development of novel methods for the environmentally benign and selective construction of C=N bonds.[1,4] Under reductive conditions, the selective construction of C=N is very challenging, as the hydrogenation of C=N bonds into C−N bonds is both kinetically and thermodynamically favorable.[5,6] Therefore, current methods on the selective construction of C=N bonds are mainly performed under oxidative or inert atmospheres, such as the oxidation/dehydrogenation of secondary amines,[7,8] the dimerization of primary amines,[3] and the oxidative coupling of alcohols with anilines.[4]

From the viewpoints of green and sustainable chemistry, it is highly desirable to use renewable raw materials, such as biomass, to replace fossil resources for the synthesis of value-added products.[9−12] Alcohols, which can be generated from renewable biomass either by a chemical or biotechnology strategy,[13,14] can serve as the perfect carbon source for constructing C=N bonds. Amines and aldehydes were first obtained via the transfer hydrogenation of nitro compounds with alcohols and then coupled to generate C=N bonds (Scheme 1). Therefore, the reductive coupling of nitro compounds with biomass-derived alcohols represents the sustainable approach for the construction of C=N bonds, but it is challenging over the supported metallic nanoparticle catalysts. Considering the reductive coupling reaction on metallic nanoparticles, it proceeds via the metal-mediated "dehydrogenation−hydrogenation" mechanism (Scheme 1), involving the dehydrogenation of alcohols into carbonyl compounds to generate the active hydrogen species (M-H, metal hydride) on the surface of metallic nanoparticles, which were further used for the hydrogenation of −NO$_2$ groups into −NH$_2$ groups, followed by the condensation of amines and aldehydes into imines (C=N bonds). The adsorption of imines via π-coordination was strong on nanoparticles, leading to the facile insertion of metal hydride into the C=N bond.[15−19] In fact, the reductive coupling of nitro compounds with alcohols has been extensively studied over noble metal catalysts, but the resulting products were mainly secondary
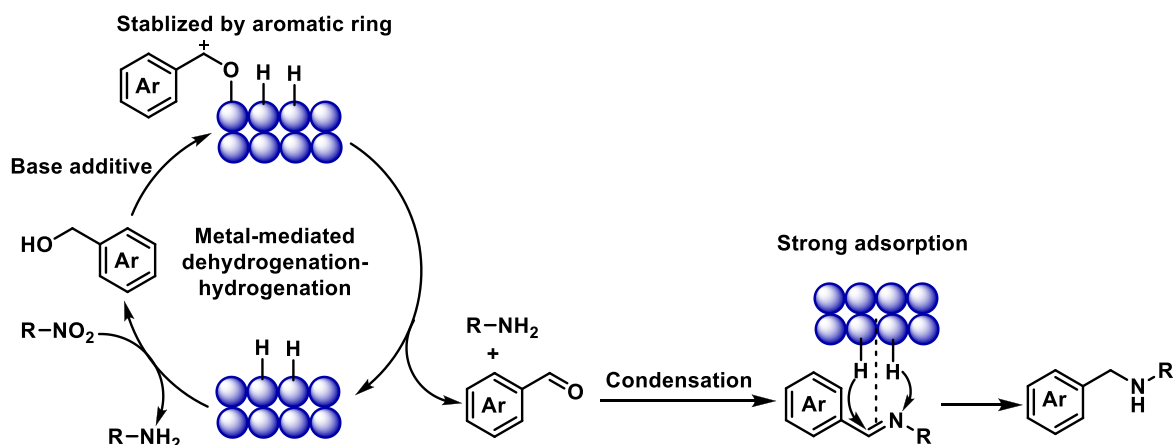
Scheme 1. Current Methods of the Reductive Coupling of Alcohols with Nitro Compounds

Previous work:

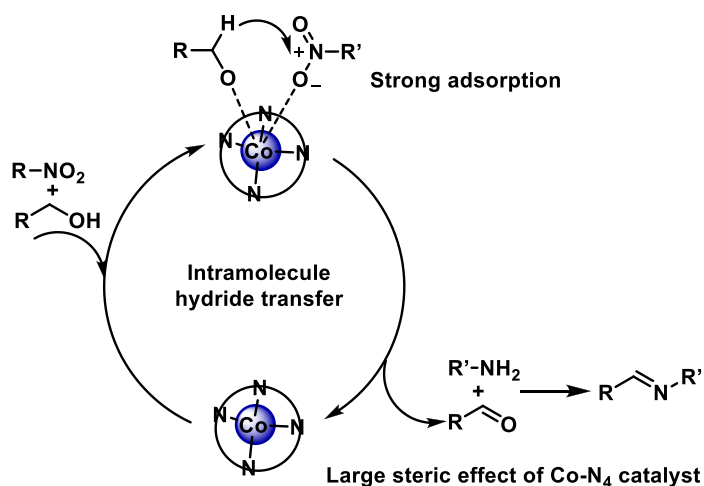### (A) Metal nanoparticle catalyzed reductive coupling

(1) Easy overhydrogenation to C-N bonds;
(2) Require base additive;
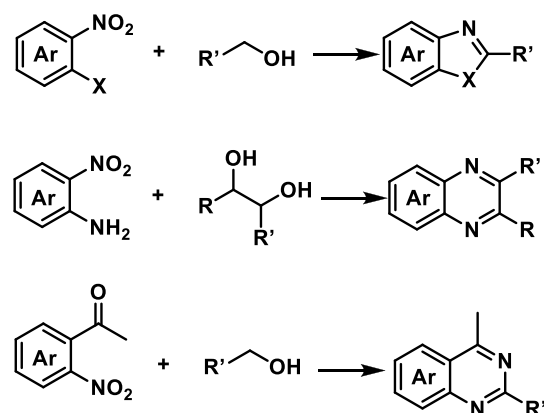(3) Limited substrate scope to active aromatic alcohol

This work:

(B) Single atom Co catalyzed reductive coupling

(C) Application in the synthesis of heterocycles

Advantages:
(1) High activity and selectivity with non-noble metal catalysts at base-free conditions
(2) Broad substrate scope including aliphatic alcohol

amines with C−N bonds (Scheme 1, reaction A), while limited cases were on the synthesis of imines with C=N bonds.[6,16] Besides the challenge in selectivity control for C=N bonds, the limited substrate scope only included active alcohols, and the requirement for base additives to help cleave the O−H bond also impeded the industrial application of the reductive coupling strategy for C=N bond construction. To address the above-mentioned issues, it is highly demanded to design novel heterogeneous non-noble metal catalysts with high activity and selectivity for base-free C=N bond construction via the reductive coupling of nitro compounds and alcohols, especially the inert aliphatic ones.[1,20]

Reducing the affinity of imines to the catalyst surface should be an efficient way to avoid further hydrogenation of C=N bonds in imines and realize the selective synthesis of C=N bonds. It was reported that the product selectivity can be tuned by controlling the size of metal nanoparticles.[21,22] For example, Jiarui et al. reported that the selectivity of hydrogenation of 3-nitrostyrene could be controlled by manipulating the size of Pt nanoparticles in Pt/TiO₂ catalysts.[23] When the particle size was smaller than 5.5 nm, 3-vinylaniline was the main product without the hydrogenation of the vinyl group (C=C bond). If the particle size was larger than 5.5 nm, 3-ethylaniline became the major product. The authors attributed this particle-size-
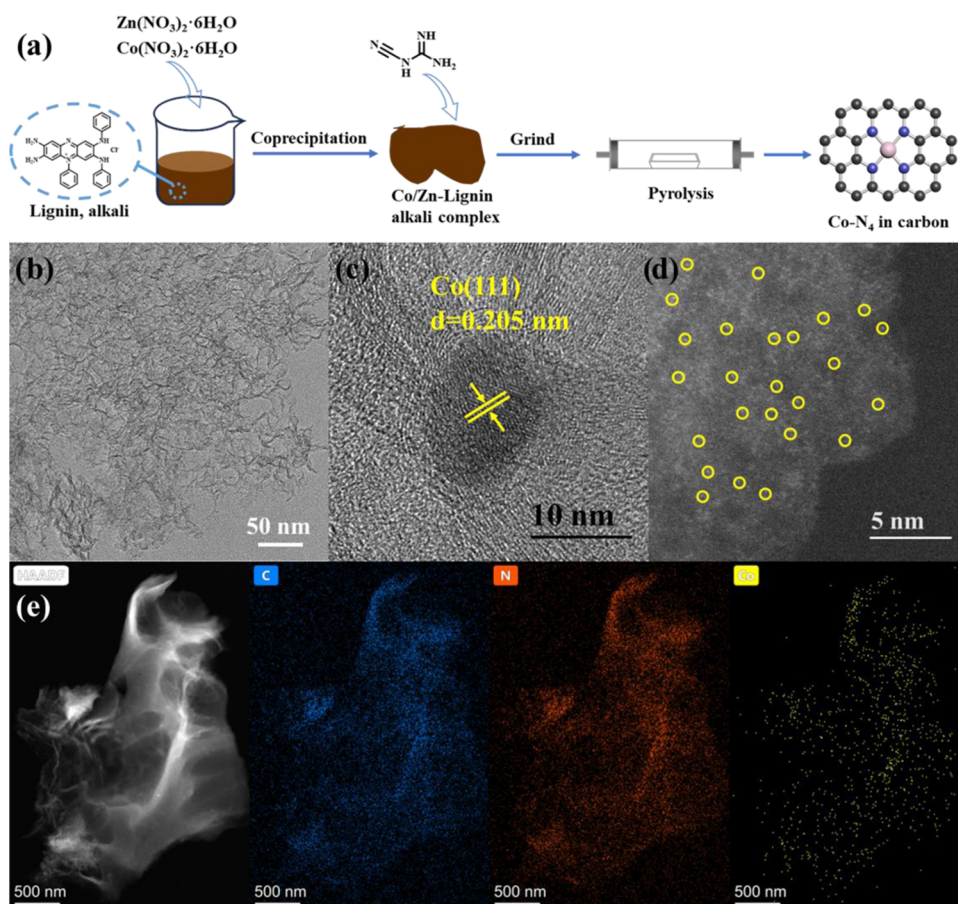
Figure 1. Preparation and characterization of Co−N$_4$/NC-1000 and Co/NC-1100 catalysts: (a) procedure of the preparation of the Co−N$_4$/NC-1000 catalyst; (b) TEM image for the Co−N$_4$/NC-1000 catalyst, and (c) HR-TEM image for the Co/NC-1100 catalyst; (d) AC-STEM image, scale bar: 5 nm; (e) HAADF-STEM image, and (f) corresponding EDX elemental mapping images of the elements C, N, and Co for the Co−N$_4$/NC-1000 catalyst, scale bar: 500 nm.

controlled selectivity to the selective adsorption of polarized nitro groups for small-sized nanoparticles. Considering the similar chemical environment and electronic property of the C=N bonds in imines and the C=C bond in 3-nitrostyrene, it is expected that reducing the size of nanoparticles would be an effective way for the selective synthesis of imines by the reductive coupling of nitro compounds and alcohols. Unlike the challenge in the preparation of small-sized noble metal nanoparticles, it is difficult to prepare small-sized non-noble metal nanoparticle catalysts (<5.0 nm) with enhanced catalytic activity and high stability in the reductive coupling of nitro compounds and alcohols, especially aliphatic ones.

Besides metal nanoparticles, single metal atom catalysts have emerged as a new frontier in the field of heterogeneous catalysis because of their high atom utilization and unique properties.[24−28] In recent years, our group has successfully prepared several kinds of nitrogen-coordinated single-atom metal catalysts for some important chemical reactions.[29−31] The single metal atom sites were discovered to play multiple roles in the activation of substrates via the Lewis acid−Lewis base interaction or mediating the electron transfer.[29] Based on our previous experiences, it is expected that the single metal atoms might activate alcohols via Lewis acid−Lewis base interaction for reductive coupling with nitro compounds. Meanwhile, the C=N bonds in the aimed imine products should desorb off from the catalyst surface due to the large steric hindrance, avoiding further hydrogenation of C=N

bonds (Scheme 1, reaction B, right). Herein, the single-atom Co catalyst bearing with Co−N$_4$ motifs was successfully prepared by the simple pyrolysis method, and it demonstrated an excellent catalytic performance for the selective construction of C=N bonds toward the additive-free synthesis of structure-diverse imines and N-heterocycles, including benzazoles, quinoxalines, and quinazolines via the reductive coupling of nitro compounds with alcohols for the first time (Scheme 1, reaction C).

RESULTS AND DISCUSSION

Catalyst Preparation and Characterization

As shown in Figure 1a, the biomass-derived lignin alkali was used as the polymer precursors to host Co^{2+} and Zn^{2+} cations via the coordination with nitrogen atoms in lignin alkali. To further increase the content of nitrogen atoms in the catalyst, dicyandiamide was mixed with a Co/Zn-lignin alkali complex, and the composite was subjected to pyrolysis under the flow of nitrogen gas. Zn atoms were introduced into the starting materials (Co/Zn-lignin alkali) to increase the spatial distance of cobalt atoms and avoid the aggregation of single Co atoms in the formation of Co nanoparticles or clusters. As the boiling point of Zn was 908 °C,[32] two pyrolysis temperatures of 1000 and 1100 °C were selected in order to fully evaporate off the Zn atoms in the as-prepared Co catalysts, which were abbreviated as Co−N$_4$/NC-1000 and Co/NC-1100, respec-
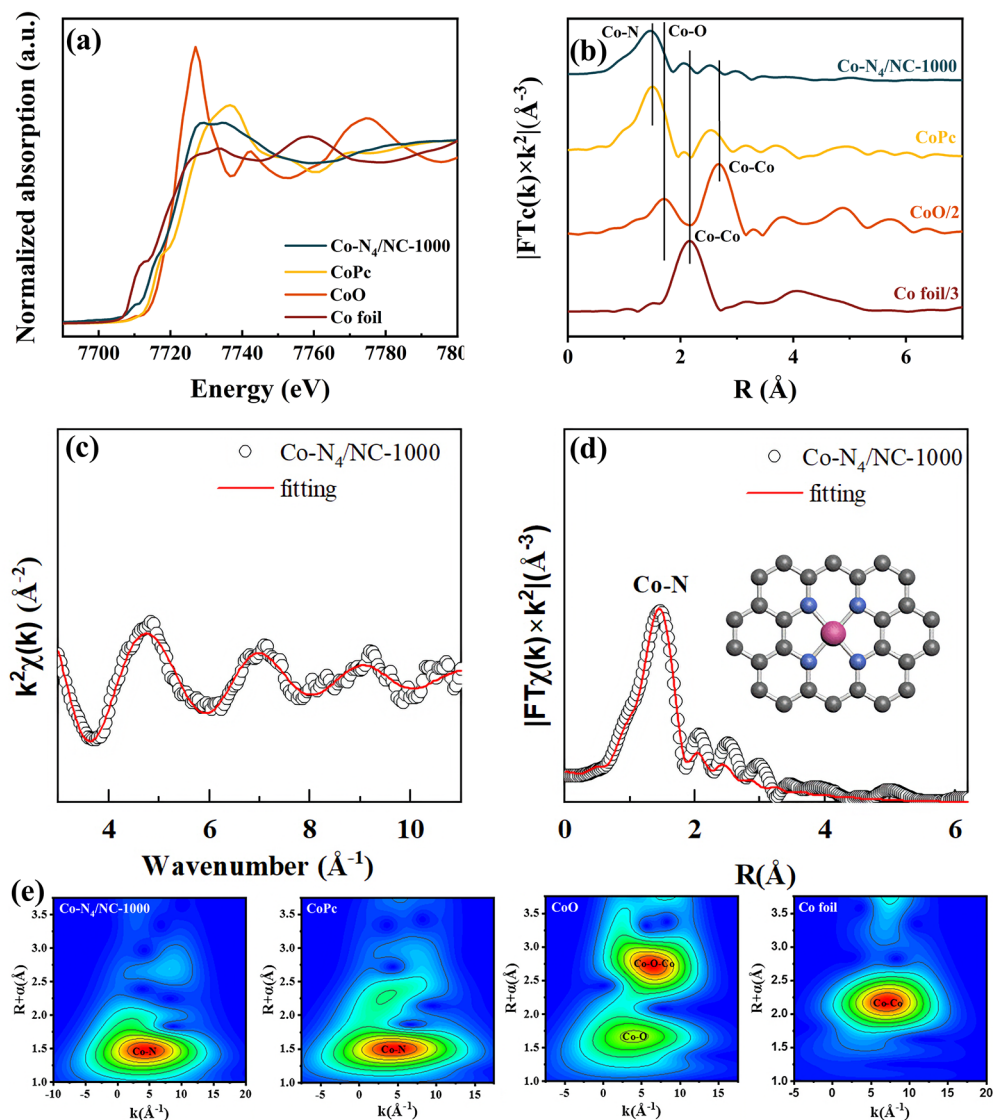
Figure 2. (a) Co K-edge XANES spectra of Co−N$_4$/NC-1000, CoPc, CoO, and Co foil. (b) The corresponding Fourier-transformed (FT) k^3-weighted Co K-edge spectra obtained on Co−N$_4$/NC-1000, CoPc, CoO, and Co foil. (c, d) The corresponding XAFS fitting curves of Co−N$_4$/NC-1000 in k (c) and R (d) space, the inset shows the schematic model of the Co−N$_4$ moiety in the carbon framework. (e) Wavelet transformation (WT) for the k^3-weighted Co K-edge XAFS signal of Co−N$_4$/NC-1000, CoPc, CoO, and Co foil (from left to right).

tively, according to the following characterization. Indeed, the mass content (wt %) of Co in the two Co catalysts was determined by inductively coupled plasma atomic emission spectroscopy (ICP-AES) to be 2.7 and 3.5 wt % for Co−N$_4$/NC-1000 and Co/NC-1100, respectively, while Zn was below the detection limit (10^{-3} wt %). Compared with Co−N$_4$/NC-1000, the higher weight percentage of Co in Co/NC-1100 was due to the release of many more volatile compounds at the higher pyrolysis temperature of 1100 °C. NC-1000 was prepared with a method similar to that for Co−N$_4$/NC-1000 except that no Co source was added.

X-ray diffraction (XRD) pattern of Co−N$_4$/NC-1000 only showed a broad shoulder peak at 26.4° and a weak peak at 42.4° (Figure S1), assigning to the (002) and (100) planes of the graphitic carbon, respectively (PDF #89-8487).[33,34] However, besides the graphitic peaks, an additional peak at 44.2° is observed in the XRD pattern of Co/NC-1100, attributing to the characteristic (111) facet of metallic Co nanoparticles (JCPDS PDF#15−0806).[6] According to the

XRD results, it can be concluded that the Co species in Co−N$_4$/NC-1000 should be present as single Co atoms or Co clusters. Transmission electron microscopy (TEM) was also conducted to identify the morphologies and presence of Co species in the two catalysts. As shown in Figure 1b, the thin nitrogen-doped carbon layers were observed in the high-resolution TEM (HR-TEM) image of Co−N$_4$/NC-1000 without the observation of cobalt nanoparticles or tiny clusters. While cobalt nanoparticles were clearly observed in the TEM image of Co/NC-1100 with an average size of 15.8 nm (Figure S2), a lattice fringe of 0.205 nm corresponding to the (111) facet of Co was found in the HR-TEM image (Figure 1c), in good accordance with the XRD results. Then, we resorted to aberration-corrected high-angle annular dark-field scanning transmission electron microscopy (AC HAADF-STEM) to identify the Co species in Co−N$_4$/NC-1000. As shown in Figure 1d, single Co atoms were atomically dispersed on the nitrogen-doped carbon under a high magnification mode and were marked by separated bright dots and highlighted by

yellow circles. HAADF-STEM image and the corresponding EDX elemental mapping images of Co−N$_4$/NC-1000 revealed that elements of N and Co were homogeneously distributed on the entire carbon support (Figure 1e,f).

X-ray photoelectron spectroscopy (XPS) was used to detect the valence states of the *as*-prepared Co catalysts. After careful fitting, a significant difference was observed in the Co 2p XPS spectra of Co−N$_4$/NC-1000 and Co/NC-1100. The fitted Co 2p$_{3/2}$ XPS spectrum of Co−N$_4$/NC-1000 showed a main peak at a binding energy of 780.5 eV and a satellite peak with a binding energy of 784.2 eV, which suggests that the surface valence state of Co in Co−N$_4$/NC-1000 was close to +2 (Figure S3a). The two main peaks with binding energies at 779.4 and 781.0 eV were observed for the fitted Co 2p$_{3/2}$ XPS spectrum of Co/NC-1100 (Figure S3b), assigned to the metallic Co and oxidized Co species, respectively. The presence of oxidized Co species in Co/NC-1100 is due to the surface oxidation of metallic Co during the storage of the catalyst in the air.[20] The XPS results revealed that metallic Co^0 was only present in Co/NC-1100, in good accordance with the XRD and TEM results (Figures S1 and S2). Considering the N 1s XPS spectra, five peaks were fitted for Co−N$_4$/NC-1000 and Co/NC-1100 (Figure S4) with different binding energies as follows: pyridinic N (398.7 eV), Co−N$_x$ (399.7 eV), pyrrolic N (401.0 eV), graphitic N (402.7 eV), and oxidized N (405.2 eV).[35] The atomic percentage (atom %) of nitrogen atoms determined by XPS was noted to decrease greatly from 13.4 atom % in Co−N$_4$/NC-1000 to 5.0 atom % in Co/NC-1100, suggesting that a large amount of nitrogen species were released at 1100 °C (Table S1). In addition, the pyridinic N atoms, which are generally believed to be the anchoring sites to the single metal atoms,[36] were the major N species in Co−N$_4$/NC-1000 with an atomic percentage up to 46.9 atom %.

Furthermore, X-ray absorption near-edge structure (XANES) and X-ray absorption fine structure (XAFS) analyses were performed to reveal the local coordination environment and chemical state of the single Co atoms in Co−N$_4$/NC-1000. The E$_0$ value (the first inflection point on the edge; the higher E$_0$, the higher oxidation state) in the XANES spectrum of Co−N$_4$/NC-1000 is located between CoO and cobalt phthalocyanine (CoPc) and far away from the Co foil (Figure 2a). These results suggest that the valence state of the single Co atom in Co−N$_4$/NC-1000 is near +2.[37] The Fourier-transformed (FT) k^3-weighted extended XAFS (EXAFS, Figure 2b) spectrum of Co−N$_4$/NC-1000 only shows a main peak at 1.88 Å, corresponding to the primary coordination shell of Co, and it is very close to the Co−N bond in CoPc but much smaller than 2.17 Å (Co−Co) found in Co foil and 2.12 Å (Co−Co) found in CoO, indicating that Co most likely coordinated N. EXAFS fitting was further performed to confirm the structural parameters and extract the quantitative chemical configuration of single Co atom. The corresponding EXAFS fitting curves of Co−N$_4$/NC-1000 in the k and R spaces are shown in Figure 2c,d, respectively. The best fitting result for the first shell shows that each Co atom is coordinated with four nitrogen atoms on average with a Co−N$_4$ motif (Table S2), and the schematic model of the Co−N$_4$ moiety in Co−N$_4$/NC-1000 is inserted in Figure 2d. EXAFS wavelet transform (WT) analysis, which can provide both radial distance resolution and wavenumber (k)-space resolution,[38] was employed to further ascertain the atomic Co dispersion. The WT EXAFS plot of Co−N$_4$/NC-1000 exhibited only one intensity maximum at ~4.6 Å^{-1} (Figure 2e), far from the value
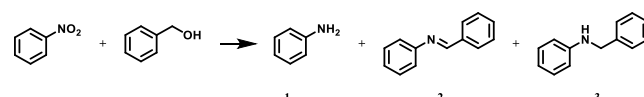
found on Co foil (7.2 Å^{-1}, Co−Co) and CoO (4.2 Å^{-1}, Co−O) but very close to the value found on CoPc. Thus, the Co species in Co−N$_4$/NC-1000 were confirmed to be atomically distributed and coordinated with N. These structural features together evidenced that the atomic isolated Co−N$_4$ sites were the only Co species in the Co−N$_4$/C-1000 catalyst.

Finally, the texture properties of the *as*-prepared Co catalysts were investigated by N$_2$ adsorption−desorption isotherms. As shown in Figure S5, the N$_2$ adsorption−desorption isotherms of the two catalysts displayed a type-IV isotherm with an H4 hysteresis loop and an I-type isotherm with equilibrium in the P/P_0 range 0−0.1, which were characteristics of micro/mesoporous materials. Pore size distributions also revealed a wide distribution in pore sizes with both micropores and mesopores in the two catalysts. Due to the evaporation of Zn atoms and the release of volatile gases, Co−N$_4$/NC-1000 and Co/NC-1100 have a similar large surface area up to 826.9 and 923.7 m^2/g (Table S3), respectively.

Catalyst Screening and Optimization of the Reaction Conditions

The reductive coupling of nitrobenzene with benzyl alcohol was used as the model reaction to evaluate the catalytic performance of the *as*-prepared Co catalysts (Table 1). To our
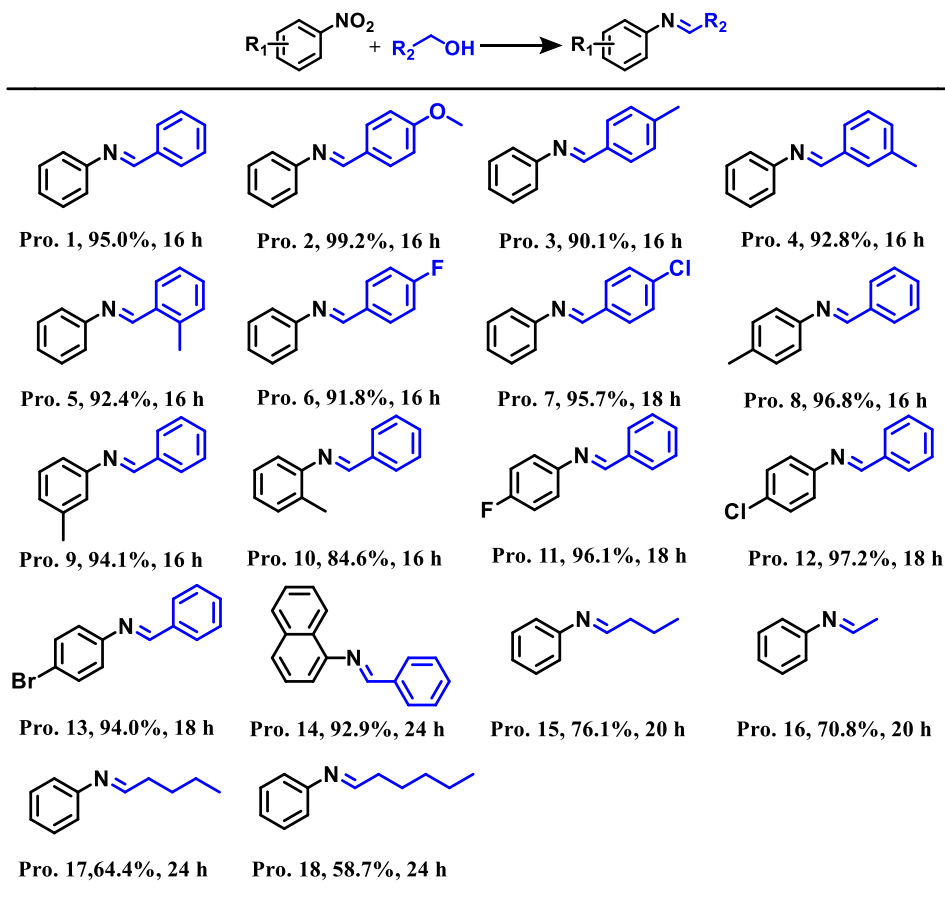
Table 1. Catalyst Screening for Aerobic Ammoxidation of Benzaldehyde[a]

entry	catalyst	conversion (%)	selectivity (%)		
			1	2	3
1	Co−N$_4$/NC-1000	60.9	3.0	95.9	1.1
2	Co/NC-1100	4.8	13.0	87.0	0.0
3	NC-1000	<1	>99		
4	Pt/C	59.0		82.2	17.8
5	Pd/C	32.0		86.9	13.1
6[c]	Co−N$_4$/NC-1000	11.9	18.0	80.9	1.1
7[d]	Co−N$_4$/NC-1000	7.8	25.0	73.6	1.4
8[e]	Co−N$_4$/NC-1000	>99	1.3	95.0	2.4

[a]Reaction conditions: Nitrobenzene (0.5 mmol), metal loading (1.8 mol %), 180 °C, hexane (10 mL), and 8 h. [b]20 mg of NC-1000 was used. [c]KSCN (0.5 mmol) was added. [d]Pyrrole (0.5 mmol) was added. [e]Reaction time was prolonged to 16 h.

great pleasure, Co−N$_4$/NC-1000 demonstrated an excellent catalytic performance for this transformation, which gave a 60.9% conversion of nitrobenzene at 180 °C after 8 h (Table 1, entry 1). In contrast to Co−N$_4$/NC-1000, Co/NC-1100 bearing Co metallic nanoparticles demonstrated much lower activity, affording a lower conversion of 4.8% (Table 1, entries 1 vs 2). Cobalt-free nitrogen-doped carbon (abbreviated as NC-1000) was also prepared by the same procedure as that for Co−N$_4$/NC-1000 except that cobalt salt was not added in the precursor. NC-1000 delivered almost no activity in this reaction (Table 1, entry 3), indicating that nitrogen-doped carbon was not active in this transformation. These results confirmed that single-atom Co−N$_4$ motifs instead of metallic Co nanoparticles were the active sites for the reductive coupling reactions. As expected, the poisoning experiment by KSCN resulted in a great decrease in nitrobenzene conversion because of the strong affinity of SCN$^-$ to the single metal

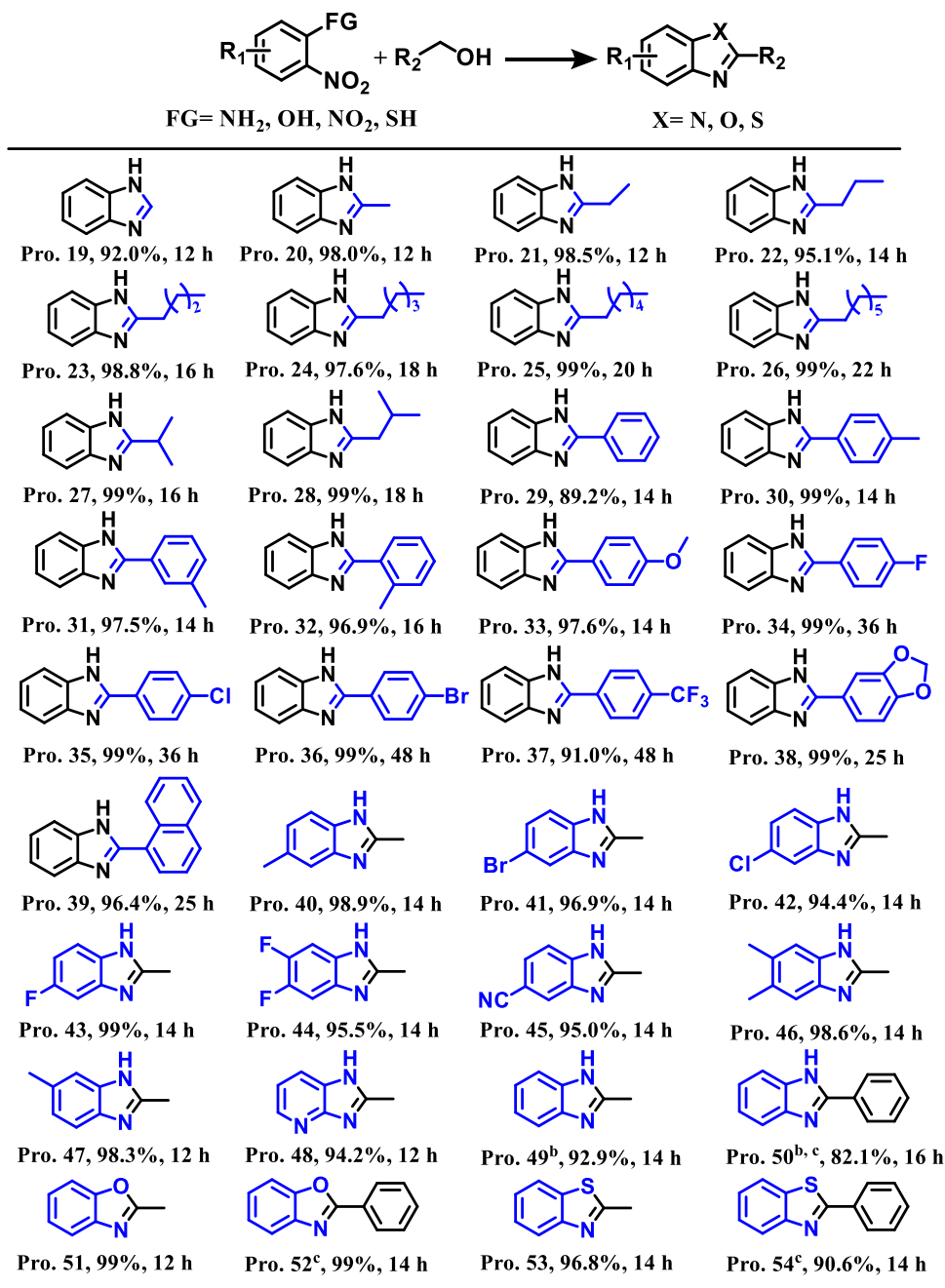**Table 2. Synthesis of Imines with Alcohols and Nitro Compounds**[a]

Pro. 1, 95.0%, 16 h   Pro. 2, 99.2%, 16 h   Pro. 3, 90.1%, 16 h   Pro. 4, 92.8%, 16 h

Pro. 5, 92.4%, 16 h   Pro. 6, 91.8%, 16 h   Pro. 7, 95.7%, 18 h   Pro. 8, 96.8%, 16 h

Pro. 9, 94.1%, 16 h   Pro. 10, 84.6%, 16 h   Pro. 11, 96.1%, 18 h   Pro. 12, 97.2%, 18 h

Pro. 13, 94.0%, 18 h   Pro. 14, 92.9%, 24 h   Pro. 15, 76.1%, 20 h   Pro. 16, 70.8%, 20 h

Pro. 17, 64.4%, 24 h   Pro. 18, 58.7%, 24 h

[a]Reaction conditions: Nitroarenes (0.5 mmol), Co−N$_4$/NC-1000 (20 mg), hexane (10 mL), aromatic alcohols (3 mmol), 180 °C and N$_2$ (10 bar); Note: aliphatic alcohols were also used as the reaction solvents.

atoms (Table 1, entries 6).[29,39] It was noted that Co−N$_4$/NC-1000 even demonstrated comparable activity to Pt/C and much higher catalytic activity than Pd/C (Table 1, entries 1 vs 4 and 5) under identical conditions. The reaction route was then investigated. Generally, two mechanisms have been reported for transfer hydrogenation with alcohol: (1) metal-mediated dehydrogenation−hydrogenation and (2) intramolecular hydride transfer.[40] Transfer hydrogenation over metallic nanoparticle catalyst normally proceeded via mechanism 1 with the formation of metal hydride as the active species.[41] Considering the oxidation states of Co and low concentration of Co sites, the reductive coupling of nitrobenzene with benzyl alcohol over the Co−N$_4$/NC-1000 catalyst was more likely to proceed via the intramolecular hydride transfer mechanism. Controlled experiments on the dehydrogenation of benzyl alcohol performed over Pd/C and Co−N$_4$/NC-1000 catalysts also confirmed distinct mechanisms over these two catalysts. The dehydrogenation of benzyl alcohol over Pd/C gave 15.3% conversion after 8 h at 180 °C, while Co−N$_4$/NC-1000 showed no activity in the dehydrogenation of benzyl alcohol (Table S4).

Besides the superior high catalytic activity of Co−N$_4$/NC-1000 over Pd/C and Pt/C catalysts, Co−N$_4$/NC-1000 also demonstrated a great advantage in the achievement of high selectivity of imines with C=N bonds. The imine molecules can adsorb on the surface of the metallic Pd or Pt nanoparticles by π-coordination via the C=N bonds, leading to the

inevitable insertion of metal hydride into the C=N bonds.[42] However, the hydrogenation of the C=N bonds was much more difficult over Co−N$_4$/NC-1000 due to the prohibited π-coordination adsorption from large hindrances and the absence of metal hydride species. Electron-rich alkoxides from deprotonation of alcohols (RCH$_2$OH) and nitro group should have a stronger interaction with the electron-deficient Co$^{\delta+}$ site, while the weak polar C=N bonds bound weakly to Co−N$_4$ sites in Co−N$_4$/NC-1000 due to large steric hindrance from bulky substituents on C and N atoms. The above discussion was also confirmed by DFT calculations (*vide infra*).

Another key advantage of our developed Co−N$_4$/NC-1000 catalysts was the fact that they were free of base-free conditions. Base additives were generally required for metallic nanoparticle-catalyzed reductive coupling reactions to help capture H$^+$ from the −OH group in alcohols and form alkoxide anions (RCH$_2$O$^-$) and metal hydride for the hydrogenation of −NO$_2$ groups.[5,6,43] The as-prepared Co−N$_4$/NC-1000 catalyst has abundant basic N atoms (particularly, pyridinic N) (Table S1), avoiding the use of external base additives.[44] The amount of basic sites was determined to be 0.394 and 0.170 mmol/g for Co−N$_4$/NC-1000 and Co/NC-1100 by CO$_2$ temperature-programmed deposition (CO$_2$-TPD) profile, respectively (Table S5, Figure S6). The larger amount of basic sites in Co−N$_4$/NC-1000 compared to Co/NC-1100 was due to its larger content of nitrogen atoms. Lower conversion obtained

Table 3. Reductive Coupling of Alcohols with Two-Substituted Nitrobenzenes[a]

FG= NH$_2$, OH, NO$_2$, SH   X= N, O, S

Pro. 19, 92.0%, 12 h	Pro. 20, 98.0%, 12 h	Pro. 21, 98.5%, 12 h	Pro. 22, 95.1%, 14 h
Pro. 23, 98.8%, 16 h	Pro. 24, 97.6%, 18 h	Pro. 25, 99%, 20 h	Pro. 26, 99%, 22 h
Pro. 27, 99%, 16 h	Pro. 28, 99%, 18 h	Pro. 29, 89.2%, 14 h	Pro. 30, 99%, 14 h
Pro. 31, 97.5%, 14 h	Pro. 32, 96.9%, 16 h	Pro. 33, 97.6%, 14 h	Pro. 34, 99%, 36 h
Pro. 35, 99%, 36 h	Pro. 36, 99%, 48 h	Pro. 37, 91.0%, 48 h	Pro. 38, 99%, 25 h
Pro. 39, 96.4%, 25 h	Pro. 40, 98.9%, 14 h	Pro. 41, 96.9%, 14 h	Pro. 42, 94.4%, 14 h
Pro. 43, 99%, 14 h	Pro. 44, 95.5%, 14 h	Pro. 45, 95.0%, 14 h	Pro. 46, 98.6%, 14 h
Pro. 47, 98.3%, 12 h	Pro. 48, 94.2%, 12 h	Pro. 49[b], 92.9%, 14 h	Pro. 50[b, c], 82.1%, 16 h
Pro. 51, 99%, 12 h	Pro. 52[c], 99%, 14 h	Pro. 53, 96.8%, 14 h	Pro. 54[c], 90.6%, 14 h

[a]Reaction conditions: 2-OH/NH$_2$/NO$_2$/SH nitrobenzene (0.5 mmol), the Co−N$_4$/NC-1000 catalyst (20 mg), hexane (10 mL), aromatic alcohols (3 mmol), and 180 °C. [b]1,2-Dinitrobenzene was used as the substrate. [c]6 mmol of benzyl alcohol was used. Note: Aliphatic alcohols were also used as the reaction solvents.

in the presence of the acidic pyrrole molecules also confirmed the crucial role of basic nitrogen atoms in the Co−N$_4$/NC-1000 catalyst (Table 1, entries 1 vs 7).

It was noted that the reductive coupling of nitrobenzene with benzyl alcohol was greatly affected by the reaction solvents (Table S6). Hexane and toluene without heteroatoms were much better than other solvents, affording high nitrobenzene conversions of 60.9 and 56.7%, respectively. However, poor or low nitrobenzene conversions (3.7−32.9%) were attained in the solvents containing nitrogen or oxygen atoms, such as 1,4-dioxane, tetrahydrofuran (THF), and acetonitrile. The possible reason should be the strong affinity

of these solvents to single Co atom sites by the interaction of the heteroatoms in these solvents with the single Co atoms, similar to the decrease in the activity of Co−N$_4$/NC-1000 by the addition of KSCN as described above (Table 1, entries 1 vs 6). By prolonging the reaction time to 16 h, N-benzylideneaniline attained a high yield of 95.0% with full nitrobenzene conversion (Table 1, entry 8).

Then, the substrate scope for the synthesis of imines was studied. As shown in Table 2, structure-diverse imines with high to excellent yields (70.8% ∼ 99.2%) were successfully produced via the reductive coupling of nitroarenes with alcohols over Co−N$_4$/NC-1000. Compared with the reactions

with aromatic alcohols, the reductive coupling of nitrobenzene with aliphatic alcohols produced the corresponding imines with relatively low yields (Pro. 1−14 vs Pro. 15−18) due to the presence of side byproducts. C1−C4 alcohols can undergo the carbon-chain growth side reactions between the alcohols and the *in situ* formed aldehydes to generate the long-chain compounds, which couple with the *in situ* formed anilines to reduce the yields of the corresponding imines.[45,46] For example, 10.6% 2-methyl-quinoline was produced in the reductive coupling of nitrobenzene and ethanol.

Generally, reductive coupling of aliphatic alcohols and nitro compounds was quite difficult due to the challenge in the dehydrogenation of aliphatic alcohols. The superior catalytic activity of Co−N$_4$/NC-1000 over metallic nanoparticle catalysts, such as Pt/C and Pd/C, may be due to the different reaction mechanisms. The key step in the metal-mediated transfer hydrogenation, the major mechanism over supported metallic nanoparticles, was the generation of active H species through the dehydrogenation of alcohols (RCH$_2$OH), which were further used for *in situ* reduction of the nitro group. Such a mechanism was greatly affected by the stability of the carbocation after removing α-C$_{sp3}$-H (RCH$^+$OH). Therefore, the transfer hydrogenation of aromatic alcohols was much easier than the aliphatic alcohols over metallic nanoparticles due to the enhanced stabilization effect on the carbocation from the aromatic ring,[41,47] and most of the reported methods were only suitable for the active aromatic alcohols.[6,48,49] While for Co−N$_4$ sites in Co−N$_4$/NC-1000, the single-atom Co$^{\delta+}$ sites in Co−N$_4$/NC-1000 could activate alcohols via Lewis acid−Lewis base interaction and promote the transfer of the H atoms in alcohols to the −NO$_2$ group directly. The reaction started from the strong adsorption of ethanol on the Co$^{\delta+}$ site, following the abstraction of the proton from O−H by adjacent N, while the Lewis acid Co$^{\delta+}$ site coordinated with the alkoxide ion (conjugated base of alcohol). The transfer of the H atom from the α-C$_{sp3}$-H to the −NO$_2$ group and generation of aldehyde then proceeded in a coordinated manner without carbocation formation. Therefore, the R groups in alcohols should not influence the activity of the substrates. That was why aliphatic alcohols, which should be inert over nanoparticle catalysts, were active in our method.

Substrate Scope for the Synthesis of Benzazoles

The success in the selective synthesis of imines inspired us to further extend our developed method for the synthesis of *N*-heterocycles via the reductive coupling strategy, which also involves the reductive coupling step to generate the C=N bonds. First, the synthesis of benzazoles was carried out by the reductive coupling of 2-NH$_2$/OH/SH-substituted nitrobenzene with alcohols (Table 3). The reductive coupling of 2-nitroaniline with biomass-derived alcohols was explored over the Co−N$_4$/NC-1000 catalyst. Our developed single Co atom catalytic system shows an extremely wide substrate scope. Both aliphatic (Table 3, Pro. 19−28) and aromatic alcohols (Table 3, Pro. 29−39) were suitable hydrogen donors and alkylated reagents for the reductive coupling with 2-nitroaniline, affording the corresponding 2-alkyl benzimidazoles with high to quantitative yields. The activity of the nonbranched aliphatic alcohols decreased with an increase of the carbon number (Table 3, Pro. 19−26) because aliphatic alcohols bearing longer carbon chains had larger steric hindrance to the single Co atom sites in Co−N$_4$/NC-1000. Unlike the synthesis of imines from the reductive coupling of nitrobenzene with
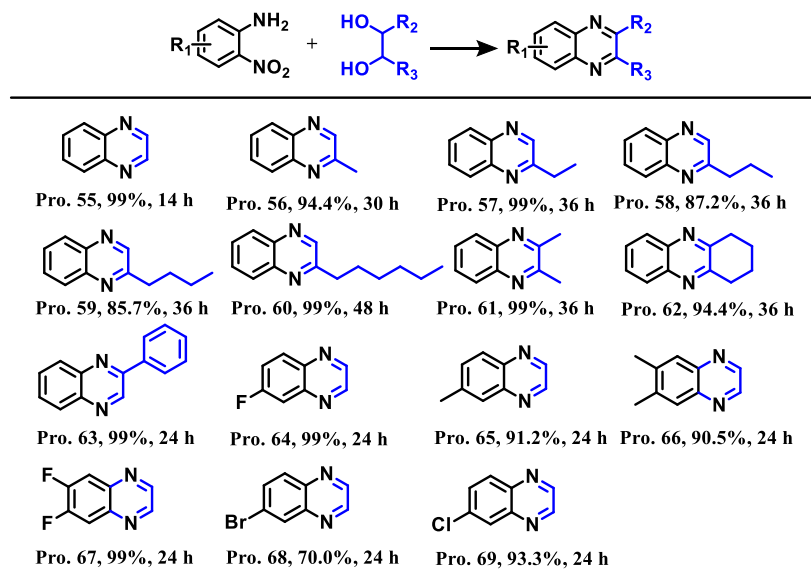
aliphatic alcohols, the reductive coupling of 2-nitroaniline with aliphatic alcohols produced the corresponding benzimidazoles with excellent yields, possibly due to the fast cyclization process, which inhibits the side reactions.

For the reductive coupling of 2-nitroaniline with aromatic alcohols, hexane was also screened to be the best solvent (Table S6). The activity of aromatic alcohols was affected by the electronic properties of the substituted groups. Aromatic alcohols with electron-donating substituted groups demonstrated higher activity than those with electron-withdrawing substituted groups (Table 3, Pro. 30−33 vs 34−37). The possible reason should be due to the fact that the electron-donating substituted groups would enhance the electron density of the α-C$_{sp3}$-H bond, which benefited the transfer of the negative H atom (H$^−$) from α-C$_{sp3}$-H to the nitro groups after the activation by a single Co atom catalyst. Compared with *p*-methyl benzyl alcohol and *m*-methyl benzyl alcohol, *o*-methyl benzyl alcohol showed steric hindrance in the reductive coupling of 2-nitroaniline (Table 3, Pro. 30−31 vs 32). The reductive coupling of fused-ring alcohols with 2-nitroaniline also proceeded smoothly, affording the corresponding benzimidazoles with excellent yields (Table 3, Pro. 38 and 39). Furthermore, various kinds of 2-nitroaniline derivatives, including the heterocyclic substrates, all successfully underwent the reductive coupling reactions with ethanol to give the corresponding 2-methyl-benzimidazole derivatives with excellent yields (Table 3, Pro. 40−48). In contrast to aromatic alcohols, the electron properties and the number of substituted groups in 2-nitroaniline derivatives showed no significant influence on the catalytic efficiency, which suggests that the cleavage of the α-C$_{sp3}$-H bonds in alcohols should be more difficult than the reduction of the nitro group by the hydrogen atoms transferred from alcohols. Besides 2-nitroanilines, 1,2-dinitrobenzene with two nitro groups was also suitable for the synthesis of benzimidazoles with aliphatic and aromatic alcohols (Table 3, Pro. 49 and 50). After the success in the synthesis of benzimidazole derivatives, the reductive coupling of 2-nitrophenol or 2-nitro thiophenol with alcohols was also conducted, affording the corresponding benzoxazoles and benzothiazoles with high to quantitative yields (Table 3, Pro. 51−54), respectively. Besides the high catalytic activity, Co−N$_4$/NC-1000 also showed good tolerance to other functional groups, such as halogen and nitrile groups, which was also one of the significant merits as compared with those of other catalytic systems. For example, the base additives generally caused the dehalogenation of halogen-substituted substrates.[50] In addition, it was noted that the side reaction of the *N*-alkylation of benzimidazole was not observed in our catalytic system. As shown in Scheme S1, the synthesis of benzimidazole derivatives included three steps: (I) the initial transfer hydrogenation of −NO$_2$ groups in 2-nitroanilines to generate −NH$_2$ groups, (II) condensation of the *in situ* formed aldehydes with −NH$_2$ groups to give the Schiff base intermediates (RNH = CR), and (III) cyclization and dehydration processes to generate benzimidazole derivatives. The disappearance of these intermediates during the reaction process (Figure S7) suggests that step I is the rate-determining step, while steps II and III should be fast.
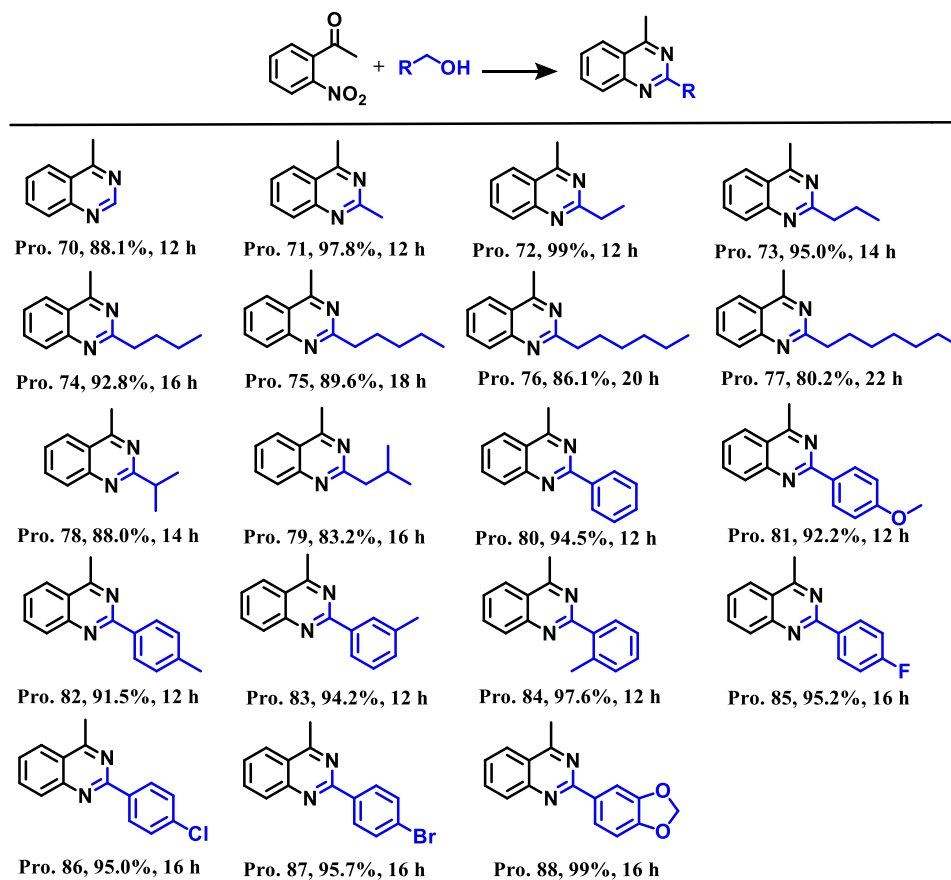
Substrate Scope for the Synthesis of Quinoxalines

Quinoxalines, as one kind of N-heterocyclic compound with two fused six-membered rings, are also very important building blocks for a variety of fine chemicals, pesticides, and

Table 4. Reductive Coupling of 2-Nitroaniline with 1,2-Diols

Pro. 55, 99%, 14 h   Pro. 56, 94.4%, 30 h   Pro. 57, 99%, 36 h   Pro. 58, 87.2%, 36 h

Pro. 59, 85.7%, 36 h   Pro. 60, 99%, 48 h   Pro. 61, 99%, 36 h   Pro. 62, 94.4%, 36 h

Pro. 63, 99%, 24 h   Pro. 64, 99%, 24 h   Pro. 65, 91.2%, 24 h   Pro. 66, 90.5%, 24 h

Pro. 67, 99%, 24 h   Pro. 68, 70.0%, 24 h   Pro. 69, 93.3%, 24 h

[a]Reaction conditions: 2-Nitroaniline (0.5 mmol), the Co−N$_4$/NC-1000 catalyst (20 mg), hexane (10 mL), 1,2-diols (5 mmol), 180 °C, and N$_2$ (10 bar). Note: Ethylene glycol was also used as the reaction solvent.

Table 5. Results of the Aromatization of 2-Nitroacetophenone with Alcohols and NH$_3$

Pro. 70, 88.1%, 12 h   Pro. 71, 97.8%, 12 h   Pro. 72, 99%, 12 h   Pro. 73, 95.0%, 14 h

Pro. 74, 92.8%, 16 h   Pro. 75, 89.6%, 18 h   Pro. 76, 86.1%, 20 h   Pro. 77, 80.2%, 22 h

Pro. 78, 88.0%, 14 h   Pro. 79, 83.2%, 16 h   Pro. 80, 94.5%, 12 h   Pro. 81, 92.2%, 12 h

Pro. 82, 91.5%, 12 h   Pro. 83, 94.2%, 12 h   Pro. 84, 97.6%, 12 h   Pro. 85, 95.2%, 16 h

Pro. 86, 95.0%, 16 h   Pro. 87, 95.7%, 16 h   Pro. 88, 99%, 16 h

[a]Reaction conditions: 2-Nitroacetophenone (0.5 mmol), Co−N$_4$/NC-1000 (20 mg), hexane (10 mL), aromatic alcohols (3 mmol), NH$_3$·H$_2$O (26.5 wt %, 200 μL),180 °C and N$_2$ (10 bar); **Note:** Aliphatic alcohols were also used as the reaction solvents.

pharmaceuticals.[51,52] The success in the synthesis of benzazoles inspired us to carry out the synthesis of quinoxalines by the reductive coupling of 2-nitroanilines and

1,2-diols over Co−N$_4$/C-1000. The reductive coupling of 2-nitroanilines with 1,2-diols also proceeded via a hydrogen atom transfer route. 1,2-Dicarbonyl compounds and o-phenylenedi-

amine intermediates were first generated by transfer hydrogenation of the nitro groups in 2-nitroanilines with 1,2-diols, and then the two intermediates condensate to produce quinoxalines (Scheme S2). As shown in Table 4, different kinds of quinoxalines were produced in high to quantitative yields from the reductive coupling of 2-nitroaniline derivatives with 1,2-diols over Co−N$_4$/NC-1000. Again, the catalytic efficiency was noted to be influenced by the structure of 1,2-diols (Pro. 55−63), while the electronic properties and the number of substituted groups in 2-nitroaniline derivatives showed no significant influence (Pro. 64−69). Similar to the decrease in the activity of nonbranched alcohols with more carbon atoms in the synthesis of benzimidazoles (Table 2, Pro. 15 and 16), the activity of 1,2-diols decreased with the increase of the carbon numbers at the C2 position due to the larger steric hindrance (Pro. 55−60).

Substrate Scope for the Synthesis of Quinazolines

Furthermore, we are also interested in the synthesis of quinazolines via the aromatization of 2-nitroacetophenone with alcohols and NH$_3$ (Table 5 and Scheme S3). Quinazolines with two nitrogen atoms in the 1,3-positions of the six-membered ring are one of the important N-heterocyclic compounds.[53] Quinazolines are widely present in natural products and synthetic pharmaceutical compounds with extensive application in the anticancer, antiviral, and antitubercular durgs.[54] Current methods for the preparation of quinazolines still suffer from some drawbacks, such as the use of expensive noble metal catalysts and relatively low atom efficiency.[55] The exploration of novel heterogeneous non-noble metal catalysts for the effective synthesis of quinazolines remains a great challenge. The excellent catalytic performance of Co−N$_4$/NC-1000 in the reductive coupling synthesis of benzazoles and quinoxalines further inspired us to explore our method for the synthesis of quinazolines via the reductive coupling of the three components, including 2-nitroacetophenone, alcohols, and NH$_3$. As expected, the aromatization of 2-nitroacetophenone with alcohols in the presence of aqueous ammonia solution over Co−N$_4$/NC-1000 proceeded smoothly at 180 °C, affording the structurally diverse quinazolines (Pro. 70−88) with high to quantitative yields (80.2% ∼ >99%). Again, this method was effective over a broad range of aromatic alcohols and inert aliphatic alcohols. For aliphatic alcohols, nonbranched aliphatic alcohols with more carbon atoms were also observed to be less active due to the steric hindrance, and a much longer reaction time was required to get high yields for the alcohols with more than three carbons (Pro. 73−77). The steric hindrance of aliphatic alcohols was also observed for the nonbranched alcohols and branched alcohols with the same carbon numbers (Pro. 73 vs Pro. 78; Pro. 74 vs Pro. 79). For aromatic alcohols, substrates with electron-donating substituted groups were more active than those with electron-withdrawing substituted groups (Pro. 81−84 vs Pro. 85−87). To the best of our knowledge, there were no reports on the use of non-noble metal catalysts for additive-free synthesis of quinoxalines via the one-pot aromatization of 2-nitroacetophenone with alcohols and NH$_3$·H$_2$O.

Considering the synthesis of quinazolines, it starts with the transfer hydrogenation of the −NO$_2$ group in 2-nitroacetophenone to the −NH$_2$ group by alcohols, followed by the condensation of the *in situ* formed aldehyde (R′CHO) and −NH$_2$ group to give the Schiff base intermediate (RNH = CR′, Scheme S3). Meanwhile, the ketone group (C═O) in 2-

nitroacetophenone undergoes condensation with the NH$_3$ molecule to generate the aldimine intermediate (RCH = NH). Furthermore, the intramolecular nucleophilic addition of the aldimine (RCH = NH) to Schiff base intermediate (RNH = CR′) produces the six-membered intermediates (Scheme S3). Finally, the dehydrogenation of one H$_2$ molecule from the six-membered intermediates gives rise to quinazolines. It should be pointed out that the cyclization process for the formation of benzazoles involves the intramolecular nucleophilic addition of the −NH$_2$ group to Schiff base intermediates (RNH = CR′) (Scheme S3). However, it was not the case for the cyclization in the synthesis of quinazolines, as the starting material, acetophenone, did not generate 1-phenyl ethylamine under the standard conditions, which indicated that the transfer hydrogenation of the C═N bonds in the aldimine intermediates (RCH = NH) was also inhibited in our catalytic systems.

Mechanism Study

After the success in a broad-range synthesis of imines and N-heterocycles with C═N bonds over Co−N$_4$/NC-1000, we give more insights into the reaction mechanism of these reductive coupling reactions. First, some controlled experiments were carried out. After the reaction, the gas phase was analyzed by gas chromatography (GC), and no H$_2$ was detected. Furthermore, the use of 1,2-diaminobenzene instead of 2-nitroaniline to couple with benzyl alcohol gave no product of 2-phenyl-benzimidazole, and the dehydrogenation of benzyl alcohol into H$_2$ and benzyl aldehyde was also not observed (Scheme S4). These results confirmed that the first step of the reduction of the nitro group in 2-nitroaniline by alcohols proceeded via the intramolecular hydride transfer route over the single Co atom sites, while that was the dehydrogenation−hydrogenation route over supported metallic nanoparticles.[6]

As discussed above, the key step toward the synthesis of N-heterocycles and imines was the transfer hydrogenation of the −NO$_2$ groups by alcohols. Therefore, the transfer hydrogenation of nitrobenzene by ethanol was used as the model reaction to study the mechanism. Considering the hydrogenation of nitrobenzene into aniline, two reaction routes have been generally accepted: "direct" route and "condensation" route (Scheme S5).[56] Both the "direct" route and the "condensation" route involve the initial hydrogenation of nitrobenzene into nitrosobenzene and the subsequent hydrogenation of nitrosobenzene into N-phenylhydroxylamine. N-phenylhydroxylamine can either be reduced to aniline directly ("direct" route) or condensate with nitrosobenzene to generate the azoxybenzene intermediate ("condensation" route), followed by the two consecutive hydrogenation routes to generate aniline.[57] No product was obtained from azobenzene, suggesting that the transfer hydrogenation of nitro groups by alcohols proceeded via the direct route over Co−N$_4$/NC-1000 (Scheme S4).

DFT calculations were then carried out to study the mechanism of the key step of the transfer hydrogenation of nitro groups by alcohols over Co−N$_4$/NC-1000, using the transfer hydrogenation of nitrobenzene with ethanol as the model reaction. A single Co atom coordinated by four nitrogen atoms (Figure S8) was constructed as the model for the Co−N$_4$/NC-1000 catalyst according to the fitting results of its EXAFS spectrum. Certainly, some nitrogen atoms without coordination with single Co atoms were also introduced into the model, considering the far more abundant nitrogen sites

(Table S1) compared to relatively low Co loading. The adsorption energies of nitrobenzene and ethanol molecules on the surface of Co−N$_4$/NC-1000 were first calculated. Results showed that ethanol had a larger adsorption energy than the nitrobenzene molecule (−0.22 vs −0.17 eV, Figure S9); thus, the ethanol molecule (CH$_3$CH$_2$OH) should preferably first adsorb on the single Co atom site via the Lewis acid−Lewis base interaction, which was also in consistence with the fact that the adsorption and activation of ethanol were the first step in the whole reaction. After adsorption, the release of the H atom (H$^+$) in the −OH group from ethanol to the nitrogen atom in the Co−N$_4$ motif was energetically unfavorable, and the energy barrier for the transfer of the H atom (H$^+$) to the unsaturated pyridinic nitrogen was calculated to be 1.37 eV (Figures S10 and 3). Interestingly, the energy barrier for the
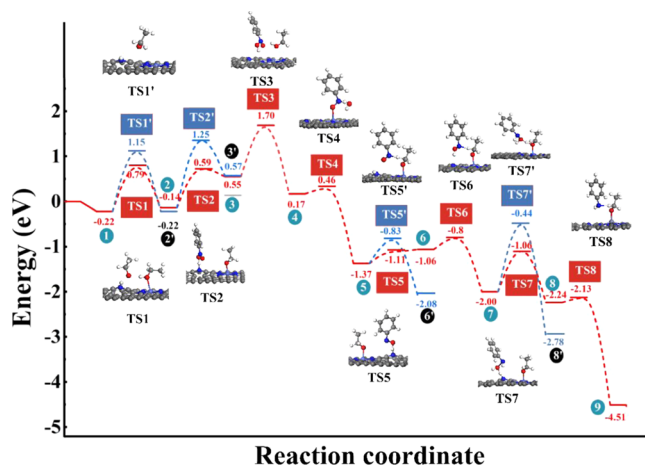
Figure 3. Energy profile and corresponding structures of nitrobenzene reduction catalyzed by catalysts.

transfer of the H atom (H$^+$) in the −OH group lowered from 1.37 to 1.01 eV with the assistance of another ethanol molecule (Figures S10 and 3), affording the active components of N−H$^+$ species and alkoxyl-Co complex (CH$_3$CH$_2$O$^-$·····Co−N$_4$). Then, the transfer hydrogenation of nitrobenzene was studied. As well-known to us, the −NO$_2$ group has the resonance structure of O=N$^+$-O$^-$, and thus the positive H atom in N−H$^+$ species and the negative H atom in α-C$_{sp3}$-H of CH$_3$CH$_2$O$^-$ should transfer to the negative oxygen atom and the positive N atom in the −NO$_2$ group, respectively. DFT calculations revealed that the energy barrier for the transfer of the first H atom from the N−H$^+$ to the −NO$_2$ group was much lower than that from α-C$_{sp3}$-H (0.73 eV vs 1.39 eV, Figure S11 & Figure 3). Thus, the reaction should start with the transfer of the positive H atom in N−H$^+$ to the negative O atom in the −NO$_2$ group to generate the PhN(O)(OH)* species (3) with the energy barrier of 0.73 eV via TS-2. Then, the transfer of the second H atom in α-C$_{sp3}$-H to PhN(O)(OH)* (3) generates the Ph-NH-(O)(OH)* species (4) with the energy barrier of TS3 in 1.15 eV (Figure 3). The further release of one water from Ph-NH-(O)(OH)* species (4) to generate the nitrosobenzene (PhNO, 5) intermediate was very easy with a low energy barrier of 0.29 eV via TS4 (Figure 3).

The transfer hydrogenation of nitrosobenzene (PhNO) into N-phenylhydroxylamine (PhNHOH) also requires the transfer of two H atoms from alcohols to PhNO, in which the H atom from the N−H$^+$ species and the H atom from -C$_\alpha$-H should transfer to the O atom and N atom in PhNO, respectively.

DFT calculations indicated that the transfer of the first H atom from N−H$^+$ species to the O atom in nitrosobenzene was much easier than that from α-C$_{sp3}$-H to the N atom in PhNO (0.26 vs 0.54 eV, Figure 3). Thus, the transformation of PhNO into PhNHOH should proceed via the transfer of the first H atom from the N−H$^+$ species to the negative O atom in PhNO to generate the PhNOH* species via TS-5 with the energy barrier of 0.26 eV, followed by the transfer of the H atom from α-C$_{sp3}$-H to the PhNOH* species to give rise to the PhNHOH intermediate via TS-6 with the energy barrier of 0.26 eV (Figure 3).

The final step of the transfer reduction of PhNHOH (7) into aniline involves the first step of the transfer of one H atom from alcohols to PhNHOH, followed by the release of H$_2$O to generate the PhNH* species. DFT calculations revealed that the energy barrier of the transfer of the H atom from −N-H$^+$ species to PhNHOH was lower than that from α-C$_{sp3}$-H to PhNHOH (0.94 vs 1.56 eV, Figure 3). Therefore, the transfer of the first H atom to PhNHOH should be from the −N-H$^+$ species via TS-7 with the energy barrier of 0.94 eV to generate the active PhNH* species with the simultaneous release of one water molecule (8, Figure 3). Finally, the transfer of the H atom from α-C$_{sp3}$-H to PhNH* species produced the final product of PhNH$_2$ via TS-8 with a low energy barrier of 0.11 eV.

In a short brief, DFT calculations revealed that the transfer hydrogenation of the nitrobenzene to PhNO is the rate-determining step with the highest energy barrier of 1.15 eV. The subsequent transfer hydrogenation of PhNO into PhNHOH was much more difficult than the final transfer hydrogenation of PhNHOH into aniline (0.26 vs 0.94 eV). As the first step of the transfer hydrogenation of nitrobenzene into PhNO has the highest energy barrier, the transfer hydrogenation of PhNO into PhNHOH as well as the transfer hydrogenation of PhNHOH into aniline should proceed quickly, in accordance with the experimental results that no intermediates were detected during the transfer hydrogenation process in Figure S7. In addition, DFT calculations revealed that the transfer of the H atom from α-C$_{sp3}$-H to the single Co atom to generate Co−H species with the simultaneous release of the acetaldehyde molecule required to overcome a high energy barrier up to 1.45 eV (Figure S12), which was much higher than the highest energy barrier (1.15 eV) for the transfer hydrogenation of nitrobenzene by ethanol. DFT calculations also revealed that the dehydrogenation of alcohols was difficult over Co−N$_4$/NC-1000, and the reduction of nitro groups by alcohols should proceed via the transfer hydrogenation strategy, in accordance with our experimental results (Scheme S4). In addition, the above DFT calculation revealed that the transfer of the H atom in -α-C$_{sp3}$-H was much more difficult than the H atom from the −OH group in alcohols via N−H$^+$ species in the rate-determining step of the transfer hydrogenation of nitrobenzene into PhNO. The kinetic isotopic effect (KIE) in the transfer reductive coupling of 2-nitroaniline using CH$_3$OD and CD$_3$OD was further studied. The KIE values of CD$_3$OD to CH$_3$OH and CD$_3$OD to CH$_3$OH were calculated to be 2.82 and 1.15 (Figure S13), respectively. By deducting the contribution of −OD from CD$_3$OD in the KIE value of CD$_3$OD to CH$_3$OH, the approximate KIE value of CD$_3$OH to CH$_3$OH should reach up to 2.67. Therefore, the results from KIE experiments also revealed that the transfer of the H atom from -α-C$_{sp3}$-H was

Scheme 2. Proposed Mechanism and Control Experiments of the Reductive Coupling of 2-Nitroaniline with Alcohols
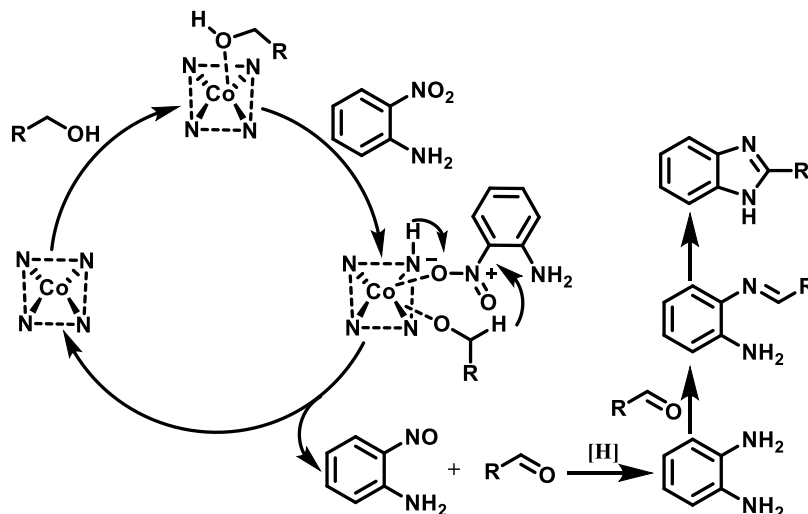
kinetically more sluggish than that from −OH in alcohols, in good accordance with the DFT calculation.

Furthermore, we are also interested in the essence of the activation of -C$_\alpha$-H in the alkoxyl group by the single Co sites. The interaction of the alkoxyl group in alcohols with single Co atom sites should be attributed to the Lewis acid−Lewis base interaction, where the single Co atoms served as the Lewis acid sites as characterized by the NH$_3$-TPD profile (Figure S6), and the oxygen atoms in the alkoxyl group were the Lewis base sites. The full inactivity or negligible activity of some representative Lewis acids, such as ZnCl$_2$, CoCl$_2$, Yb(OTf)$_3$, ZnO, AlCl$_3$, Al$_2$O$_3$, and Co$_3$O$_4$, suggested that the excellent catalytic activity of Co−N$_4$/NC-1000 in the transfer reductive coupling reactions could not be simply attributed to the Lewis acid−Lewis base interaction (Table S7). The charge distribution and the bond length of α-C$_{sp3}$-H were then calculated by DFT. As shown in Figure S14, Bader charge analysis revealed that the single Co atoms served as the electron pool to accommodate the electrons by the coordinated N atoms and then the electron with 0.500 e$^-$ transferred from Co−N$_4$/NC-1000 via single Co atoms to the adsorbed ethoxy group using the activation of an ethanol molecule as the model.

After activation of the ethoxy group by the Co−N$_4$ motif, the electron density of the H atom in -α-C$_{sp3}$-H was more negative by receiving 0.162 e$^-$. Meanwhile, the length of the -C$_\alpha$−H bond enlarged from 1.101 to 1.112 Å. These results confirmed that single Co atoms served as the bridge to transfer the electrons from the catalyst to the adsorbed alkoxyl species, resulting in the activation of the -α-C$_{sp3}$-H bond in alcohols. Thus, the transfer hydrogenation reaction became easier, especially for −NO$_2$, which has the resonance cation−anion structure (O=N$^+$-O$^-$) to assist the cleavage of α-C$_{sp3}$-H via the electronic interaction between the positive N atom in the −NO$_2$ group and a more negative H atom in α-C$_{sp3}$-H. In contrast to the −NO$_2$ group, other functional groups, including halogen, nitrile group (-−C≡N), ester (RCOOR′), vinyl group (−C=C−), alkynyl group (CH≡C−), carbonyl group (C=O) as well as the C=N bonds in imines, as listed in Table 2−5, were all well tolerated over Co−N$_4$/NC-1000, and one of the plausible reasons might be that these functional groups cannot generate the stable cation−anion structures to

assist the transfer of the negative hydrogen species (H$^+$) and positive hydrogen species (H$^-$) from alcohols to these groups.

Finally, the energy barrier of the transfer hydrogenation of C=N bonds in N-phenylethanimine into N-ethylaniline was also studied by the DFT calculation. The negative H atom from α-C$_{sp3}$-H and the positive H atom from −N-H$^+$ species should be transferred to the carbon atom and nitrogen atom in C=N bonds of imines, respectively, because of the larger electronegativity of the nitrogen atom to the carbon atom. The transfer of the first H atom from -α-C$_{sp3}$-H in the CH$_3$CH$_2$O−Co complex to the carbon atom of the C=N bond requires to overcome a high energy barrier of 1.47 eV (Figure S15). In other cases, the transfer of the first H atom from the −N-H$^+$ species to the nitrogen atom in the C=N bond in N-phenylethanimine also requires a high energy barrier of 0.34 eV (Figure S15). Therefore, DFT calculations indicated that the transfer hydrogenation of C=N bonds in imines was energetically unfavorable over the Co−N$_4$/NC-1000 catalyst, which is in good agreement with our experimental results with excellent selectivity to imines and N-heterocycles.

Based on the above DFT calculation as well as the series of controlled experiments, a plausible mechanism was proposed for the synthesis of N-heterocyclic compounds with benzazoles as the example (Scheme 2). First, the alcohols release H$^+$ from the −OH group in alcohols to generate the active alkoxy group (RCH$_2$O$^-$), where H$^+$ was captured by the basic sites of nitrogen atoms in the Co−N$_4$/NC-1000 catalyst (N−H$^+$) and RCH$_2$O$^-$ adsorbed on the surface of Co−N$_4$/NC-1000. This process is similar as the axial coordination between ligands with the metal center (M-N$_4$) in porphyrin molecules.[58] Certainly, this process can also be assigned to the Lewis acid−base interaction,[30] while the single Co atoms served as the Lewis acid sites and the nitrogen atoms as the base sites. After the activation of alcohols by single Co atom sites, the H atoms in alcohols transfer to nitro groups in 2-nitroaniline derivatives. The transfer hydrogenation of −NO$_2$ in 2-nitroaniline derivatives to −NH$_2$ by alcohols requires three consecutive transfer hydrogenation steps. Then, the condensation of −NH$_2$ with the in situ formed aldehydes gives rise to the Schiff base intermediates (RCH = NR′), followed by the ring-closing step via the nucleophilic addition to generate the dihydrobenzimidazole intermediates, and the final dehydrogenation of dihydrobenzimidazole intermediates generates benzazoles

([Scheme S1](#)). During the whole reaction pathway, the key step is the transfer hydrogenation of the nitro group step, while other steps are fast without the observation of these possible intermediates, which can even spontaneously proceed.

CONCLUSIONS

In conclusion, we have developed an effective and sustainable way for the selective synthesis of imines and *N*-heterocyclic compounds, including benzazoles, quinazolines, and quinoxalines by the reductive coupling of nitro compounds with alcohols over the single Co atom catalyst. The single Co atom catalyst was facilely prepared via pyrolysis of the biomass-derived lignin-coordinated cobalt and zinc complex with dicyandiamide as the nitrogen source. The as-prepared single Co catalyst demonstrated robust catalytic activity in the reductive coupling of nitro groups with biomass-derived alcohols to selectively construct the C≡N bonds, which was crucial for the synthesis of *N*-heterocyclic compounds and imines. The further transfer hydrogenation of C≡N bonds into C−N bonds, which required the ultrahigh energy based on DFT calculation, was not observed in our catalytic systems. The nitrogen atoms and the single Co atoms in the catalysts played synergistic roles in the activation of alcohols, where nitrogen atoms served as the base sites to combine with H^+ from alcohols, and the single Co atoms activated the alcohols to promote the transfer of the $-\alpha\text{-}C_{sp3}\text{-}H$ from alcohols to nitro groups. Our results enlarge the application of single-atom catalysts for some challenging organic transformations, which can be not readily achieved over traditional metal nano-particles.

METHODS

Materials

All of the chemicals were purchased from Aladdin Chemicals Co. Ltd. (Shanghai, China) and used as received. The alcohols with a superhigh purity were purchased from J&K Chemicals Company (Beijing, China). All other solvents were used from Sinopharm Chemical Reagent Co., Ltd. (Shanghai, China).

Catalyst Preparation

Lignin alkali (2.000 g) was first dispersed in 250 mL of deionized water with violent stirring. Then, $Co(NO_3)_2\cdot6H_2O$ (0.582 g) and $Zn(NO_3)_2\cdot6H_2O$ (2.975 g) were added to the lignin dispersion and the mixture was stirred continuously for 12 h. Finally, the Co/Zn-lignin alkali complex was separated from the reaction mixture through centrifugation and washed with distilled water several times. After overnight drying in a vacuum oven at 60 °C, the Co/Zn-lignin alkali complex was homogeneously mixed with ten times the weight of dicyandiamide by grinding in a mortar. Then, the composite was first annealed at 550 °C for 1 h and then at 1000 °C for 2 h in a tube furnace under a nitrogen atmosphere with a flow rate of 70 mL/min. After cooling to room temperature, the single Co atom catalyst was obtained, which was labeled as Co−N_4/NC-1000 according to the following structural characterization. The Co−N_4/NC-1100 catalyst was prepared with a similar method to Co−N_4/NC-1000, except that the final pyrolysis temperature was set at 1100 °C. The NC-1000 catalyst was prepared with a method similar to that of Co−N_4/NC-1000, except that Co salt was not added in the precursor.

ASSOCIATED CONTENT

S1 Supporting Information

The Supporting Information is available free of charge at https://pubs.acs.org/doi/10.1021/jacsau.3c00825.

Experimental procedure, characterization data, computational details, and NMR spectra.([PDF](#))

AUTHOR INFORMATION

Corresponding Author

Zehui Zhang − *Key Laboratory of Catalysis and Materials Sciences of the Ministry of Education, South-Central Minzu University, Wuhan 430074, P. R. China;* ⓞ orcid.org/0000-0003-1711-2191; Phone: +86-027-67842752; Email: zehuizh@mail.ustc.edu.cn; Fax: +86-411-67842752

Authors

Xixi Liu − *Key Laboratory of Catalysis and Materials Sciences of the Ministry of Education, South-Central Minzu University, Wuhan 430074, P. R. China*

Liang Huang − *The State Key Laboratory of Refractories and Metallurgy/Faculty of Materials, Wuhan University of Science and Technology, Wuhan 430074, P. R. China;* ⓞ orcid.org/0000-0001-7555-0021

Yurong He − *Key Laboratory of Catalysis and Materials Sciences of the Ministry of Education, South-Central Minzu University, Wuhan 430074, P. R. China*

Peng Zhou − *Key Laboratory of Catalysis and Materials Sciences of the Ministry of Education, South-Central Minzu University, Wuhan 430074, P. R. China;* ⓞ orcid.org/0000-0002-3317-3747

Xuedan Song − *State Key Lab of Fine Chemicals, School of Chemical Engineering, Liaoning Key Lab for Energy Materials and Chemical Engineering, Dalian University of Technology, Dalian 116024 Liaoning, P. R. China;* ⓞ orcid.org/0000-0001-7531-4344

Complete contact information is available at:
https://pubs.acs.org/10.1021/jacsau.3c00825

Author Contributions

ǁX.L., L.H., and Y.H. contributed equally to this work. X.L. and Y.H. conducted the experiment and characterizations. L.H. performed the DFT calculations. P.Z. helped discuss the project. Z.Z. designed the whole project and wrote the manuscript with contributions from other authors.

Notes

The authors declare no competing financial interest.

REFERENCES

(1) Formenti, D.; Ferretti, F.; Scharnagl, F. K.; Beller, M. Reduction of nitro compounds using 3d-non-noble metal catalysts. *Chem. Rev.* **2019**, *119* (4), 2611−2680.

(2) Schwob, T.; Kempe, R. A reusable Co catalyst for the selective hydrogenation of functionalized nitroarenes and the direct synthesis of imines and benzimidazoles from nitroarenes and aldehydes. *Angew. Chem., Int. Ed.* **2016**, *55* (48), 15175−15179.

(3) Ma, Z.; Liu, S.; Tang, N.; Song, T.; Motokura, K.; Shen, Z.; Yang, Y. Coexistence of Fe nanoclusters boosting Fe single atoms to generate singlet oxygen for efficient aerobic oxidation of primary amines to imines. *ACS Catal.* **2022**, *12* (9), 5595−5604.

(4) Shang, R.; Zhang, Q.; Lin, P.; Gu, B.; Tang, Q.; Cao, Q.; Fang, W. Aerobic activation of alcohols on Zn-promoted atomically-dispersed Ru sites encapsulated within UiO-66 framework for imine synthesis. *Appl. Catal., B* **2022**, *319*, No. 121904.

(5) Ma, S.-S.; Sun, R.; Zhang, Z.-H.; Yu, Z.-K.; Xu, B.-H. Ruthenium-catalysed chemoselective alkylation of nitroarenes with alkanols. *Org. Chem. Front.* **2021**, *8* (23), 6710−6719.

(6) Ma, Z.; Zhou, B.; Li, X.; Kadam, R. G.; Gawande, M. B.; Petr, M.; Zbořil, R.; Beller, M.; Jagadeesh, R. V. Reusable Co-nanoparticles for general and selective N-alkylation of amines and ammonia with alcohols. *Chem. Sci.* **2021**, *13* (1), 111−117.

(7) Cui, X.; Huang, Z.; van Muyden, A. P.; Fei, Z.; Wang, T.; Dyson, P. J. Acceptorless dehydrogenation and hydrogenation of N- and O-containing compounds on Pd₃Au₁(111) facets. *Sci. Adv.* **2020**, *6* (27), No. eabb3831.

(8) Gudmundsson, A.; Manna, S.; Bäckvall, J.-E. Iron(II)-catalyzed aerobic biomimetic oxidation of amines using a hybrid hydroquinone/cobalt catalyst as electron transfer mediator. *Angew. Chem., Int. Ed.* **2021**, *60* (21), 11819−11823.

(9) Espro, C.; Paone, E.; Mauriello, F.; Gotti, R.; Uliassi, E.; Bolognesi, M. L.; Rodríguez-Padrón, D.; Luque, R. Sustainable production of pharmaceutical, nutraceutical and bioactive compounds from biomass and waste. *Chem. Soc. Rev.* **2021**, *50* (20), 11191−11207.

(10) Chen, X.; Song, S.; Li, H.; Gözaydın, G.; Yan, N. Expanding the boundary of biorefinery: Organonitrogen chemicals from biomass. *Acc. Chem. Res.* **2021**, *54* (7), 1711−1722.

(11) Qi, Y.; Wang, J.; Kou, Y.; Pang, H.; Zhang, S.; Li, N.; Liu, C.; Weng, Z.; Jian, X. Synthesis of an aromatic N-heterocycle derived from biomass and its use as a polymer feedstock. *Nat. Commun.* **2019**, *10* (1), No. 2107.

(12) Jia, L.; Wang, X.; Gao, X.; Makha, M.; Wang, X.-C.; Li, Y. Tunable synthesis of furfurylamines or β-amino alcohols via Ru-catalyzed N−H functionalization using biomass-derived polyols. *Green Syn. Catal.* **2022**, *3* (3), 259−264.

(13) Gan, L.; Chidambaram, A.; Fonquernie, P. G.; Light, M. E.; Choquesillo-Lazarte, D.; Huang, H.; Solano, E.; Fraile, J.; Viñas, C.; Teixidor, F.; Navarro, J. A. R.; Stylianou, K. C.; Planas, J. G. A highly water-stable meta-carborane-based copper metal−organic framework for efficient high-temperature butanol separation. *J. Am. Chem. Soc.* **2020**, *142* (18), 8299−8311.

(14) Zheng, Y.; Zhang, R.; Zhang, L.; Gu, Q.; Qiao, Z.-A. A resol-assisted cationic coordinative Co-assembly approach to mesoporous ABO₃ perovskite oxides with rich oxygen vacancy for enhanced hydrogenation of furfural to furfuryl alcohol. *Angew. Chem., Int. Ed.* **2021**, *60* (9), 4774−4781.

(15) Hao, M.; Li, Z. Efficient visible light initiated one-pot syntheses of secondary amines from nitro aromatics and benzyl alcohols over Pd@NH₂-UiO-66(Zr). *Appl. Catal., B* **2022**, *305*, No. 121031.

(16) Cui, X.; Deng, Y.; Shi, F. Reductive N-alkylation of nitro compounds to N-alkyl and N,N-dialkyl amines with glycerol as the hydrogen source. *ACS Catal.* **2013**, *3* (5), 808−811.

(17) Xu, Y.; Zhang, Z.; Qiu, C.; Chen, S.; Ling, X.; Su, C. Photocatalytic water-splitting coupled with alkanol oxidation for selective N-alkylation reactions over carbon nitride. *ChemSusChem* **2021**, *14* (2), 582−589.

(18) Yang, H.; Cui, X.; Dai, X.; Deng, Y.; Shi, F. Carbon-catalysed reductive hydrogen atom transfer reactions. *Nat. Commun.* **2015**, *6* (1), No. 6478.

(19) Su, H.; Gao, P.; Wang, M.-Y.; Zhai, G.-Y.; Zhang, J.-J.; Zhao, T.-J.; Su, J.; Antonietti, M.; Li, X.-H.; Chen, J.-S. Grouping effect of single nickel−N₄ sites in nitrogen-doped carbon boosts hydrogen transfer coupling of alcohols and amines. *Angew. Chem., Int. Ed.* **2018**, *57* (46), 15194−15198.

(20) Senthamarai, T.; Chandrashekhar, V. G.; Rockstroh, N.; Rabeah, J.; Bartling, S.; Jagadeesh, R. V.; Beller, M. A "universal" catalyst for aerobic oxidations to synthesize (hetero)aromatic aldehydes, ketones, esters, acids, nitriles, and amides. *Chem.* **2022**, *8* (2), 508−531.

(21) Kastenmeier, M.; Fusek, L.; Deng, X.; Skála, T.; Mehl, S.; Tsud, N.; Grau, S.; Stumm, C.; Uvarov, V.; Johánek, V.; Libuda, J.; Lykhach, Y.; Mysliveček, J.; Brummel, O. Particle size and shape effects in electrochemical environments: Pd particles supported on ordered Co₃O₄(111) and highly oriented pyrolytic graphite. *J. Phys. Chem., C* **2022**, *126* (30), 12870−12881.

(22) Hayden, B. E. Particle size and support effects in electrocatalysis. *Acc. Chem. Res.* **2013**, *46* (8), 1858−1866.

(23) Zhao, J.; Fu, J.; Wang, J.; Tang, K.; Liu, Q.; Huang, J. Particle-size-dependent electronic metal−support interaction in Pd/TiO₂ catalysts for selective hydrogenation of 3-nitrostyrene. *J. Phys. Chem., C* **2022**, *126* (36), 15167−15174.

(24) Wang, X.; Zhang, Y.; Wu, J.; Zhang, Z.; Liao, Q.; Kang, Z.; Zhang, Y. Single-atom engineering to ignite 2D transition metal dichalcogenide based catalysis: Fundamentals, progress, and beyond. *Chem. Rev.* **2022**, *122* (1), 1273−1348.

(25) Bajada, M. A.; Sanjose-Orduna, J.; Di Liberto, G.; Tosoni, S.; Pacchioni, G.; Noel, T.; Vile, G. Interfacing single-atom catalysis with continuous-flow organic electrosynthesis. *Chem. Soc. Rev.* **2022**, *51* (10), 3898−3925.

(26) Zheng, X.; Liu, Y.; Yan, Y.; Li, X.; Yao, Y. Modulation effect in adjacent dual metal single atom catalysts for electrochemical nitrogen reduction reaction. *Chin. Chem. Lett.* **2022**, *33* (3), 1455−1458.

(27) Yu, L.; Huang, Q.; Wu, J.; Song, E.; Xiao, B. Spatial-five coordination promotes the high efficiency of CoN4 moiety in graphene-based bilayer for oxygen reduction electrocatalysis: A density functional theory study. *Chin. J. Chem. Eng.* **2023**, *54*, 106−113.

(28) Du, M.; Sun, Y.; Zhao, J.; Hu, H.; Sun, L.; Li, Y. Well-dispersed Mn/g-C₃N₄ as bifunctional catalysts for selective epoxidation of olefins and carbon dioxide cycloaddition. *Chin. Chem. Lett.* **2023**, *34* (12), No. 108269. DOI: 10.1016/j.cclet.2023.108269.

(29) Qin, J.; Han, B.; Liu, X.; Dai, W.; Wang, Y.; Luo, H.; Lu, X.; Nie, J.; Xian, C.; Zhang, Z. An enzyme-mimic single Fe-N₃ atom catalyst for the oxidative synthesis of nitriles via C-C bond cleavage strategy *Sci. Adv.*, 8 40 eadd1267 DOI: 10.1126/sciadv.add1267.

(30) Qin, J.; Han, B.; Lu, X.; Nie, J.; Xian, C.; Zhang, Z. Biomass-derived single Zn atom catalysts: The multiple roles of single Zn atoms in the oxidative cleavage of C−N bonds. *JACS Au* **2023**, *3* (3), 801−812.

(31) Xie, C.; Lin, L.; Huang, L.; Wang, Z.; Jiang, Z.; Zhang, Z.; Han, B. Zn-Nₓ sites on N-doped carbon for aerobic oxidative cleavage and esterification of C(CO)-C bonds. *Nat. Commun.* **2021**, *12* (1), No. 4823.

(32) Yuan, S.; Zhang, J.; Hu, L.; Li, J.; Li, S.; Gao, Y.; Zhang, Q.; Gu, L.; Yang, W.; Feng, X.; Wang, B. Decarboxylation-induced defects in MOF-derived single cobalt atom@carbon electrocatalysts for efficient oxygen reduction. *Angew. Chem., Int. Ed.* **2021**, *60* (40), 21685−21690.

(33) Lu, S.; Shi, Y.; Zhou, W.; Zhang, Z.; Wu, F.; Zhang, B. Dissolution of the heteroatom dopants and formation of ortho-quinone moieties in the doped carbon materials during water electrooxidation. *J. Am. Chem. Soc.* **2022**, *144* (7), 3250−3258.

(34) Fu, H.; Wang, B.; Zhu, D.; Zhou, Z.; Bao, S.; Qu, X.; Guo, Y.; Ling, L.; Zheng, S.; Duan, P.; Mao, J.; Schmidt-Rohr, K.; Tao, S.; Alvarez, P. J. J. Mechanism for selective binding of aromatic compounds on oxygen-rich graphene nanosheets based on molecule size/polarity matching. *Sci. Adv.* **2022**, *8* (30), No. eabn4650.

(35) Wu, W.; Zhang, Q.; Wang, X.; Han, C.; Shao, X.; Wang, Y.; Liu, J.; Li, Z.; Lu, X.; Wu, M. Enhancing selective photooxidation through Co−Nₓ-doped carbon materials as singlet oxygen photosensitizers. *ACS Catal.* **2017**, *7* (10), 7267−7273.

(36) Liu, T.; Wang, Y.; Li, Y. Two-dimensional organometallic frameworks with pyridinic single-metal-atom sites for bifunctional ORR/OER. *Adv. Funct. Mater.* **2022**, *32* (44), No. 2207110.

(37) Long, J.; Zheng, X.; Wang, B.; Wu, C.; Wang, Q.; Peng, L. Improving the electrocatalytic performances of Pt-based catalysts for oxygen reduction reaction via strong interactions with single-CoN4-rich carbon support. *Chin. Chem. Lett.* **2024**, *35*, No. 109354.

(38) Timoshenko, J.; Kuzmin, A. Wavelet data analysis of EXAFS spectra. *Comput. Phys. Commun.* **2009**, *180* (6), 920−925.

(39) Li, S.; Dong, M.; Yang, J.; Cheng, X.; Shen, X.; Liu, S.; Wang, Z.-Q.; Gong, X.-Q.; Liu, H.; Han, B. Selective hydrogenation of 5-(hydroxymethyl)furfural to 5-methylfurfural over single atomic metals anchored on Nb_2O_5. *Nat. Commun.* **2021**, *12* (1), No. 584.

(40) Gilkey, M. J.; Xu, B. Heterogeneous Catalytic Transfer hydrogenation as an effective pathway in biomass upgrading. *ACS Catal.* **2016**, *6* (3), 1420−1436.

(41) An, Z.; Yang, P.; Duan, D.; Li, J.; Wan, T.; Kong, Y.; Caratzoulas, S.; Xiang, S.; Liu, J.; Huang, L.; Frenkel, A. I.; Jiang, Y. Y.; Long, R.; Li, Z.; Vlachos, D. G. Highly active, ultra-low loading single-atom iron catalysts for catalytic transfer hydrogenation. *Nat. Commun.* **2023**, *14* (1), No. 6666.

(42) Sadeghmoghaddam, E.; Gu, H.; Shon, Y. S. Pd nanoparticle-catalyzed isomerization vs hydrogenation of allyl alcohol: Solvent-dependent regioselectivity. *ACS Catal.* **2012**, *2* (9), 1838−1845.

(43) Kozlov, A. S.; Afanasyev, O. I.; Chusov, D. Borrowing hydrogen amination: Whether a catalyst is required? *J. Catal.* **2022**, *413*, 1070−1076.

(44) Kumar, R.; Li, G.; Gallardo, V. A.; Li, A.; Milton, J.; Nash, J. J.; Kenttämaa, H. I. Measurement of the proton affinities of a series of mono- and biradicals of pyridine. *J. Am. Chem. Soc.* **2020**, *142* (19), 8679−8687.

(45) He, L.; Wang, J.-Q.; Gong, Y.; Liu, Y.-M.; Cao, Y.; He, H.-Y.; Fan, K.-N. Titania-supported iridium subnanoclusters as an efficient heterogeneous catalyst for direct synthesis of quinolines from nitroarenes and aliphatic alcohols. *Angew. Chem., Int. Ed.* **2011**, *50* (43), 10216−10220.

(46) Zhang, C.; Gao, Z.; Ren, P.; Lu, J.; Huang, Z.; Su, K.; Zhang, S.; Mu, J.; Wang, F. Oxygen-implanted MoS_2 nanosheets promoting quinoline synthesis from nitroarenes and aliphatic alcohols via an integrated oxidation transfer hydrogenation−cyclization mechanism. *Green Chem.* **2022**, *24* (4), 1704−1713.

(47) Johnstone, R. A. W.; Wilby, A. H.; Entwistle, I. D. Heterogeneous catalytic transfer hydrogenation and its relation to other methods for reduction of organic compounds. *Chem. Rev.* **1985**, *85*, 129−170.

(48) Wang, L.; Neumann, H.; Beller, M. Palladium-catalyzed methylation of nitroarenes with methanol. *Angew. Chem., Int. Ed.* **2019**, *58* (16), 5417−5421.

(49) Li, W.; Huang, M.; Liu, J.; Huang, Y.-L.; Lan, X.-B.; Ye, Z.; Zhao, C.; Liu, Y.; Ke, Z. Enhanced hydride donation achieved molybdenum catalyzed direct N-alkylation of anilines or nitroarenes with alcohols: From computational design to experiment. *ACS Catal.* **2021**, *11* (16), 10377−10382.

(50) Sahoo, B.; Surkus, A.-E.; Pohl, M.-M.; Radnik, J.; Schneider, M.; Bachmann, S.; Scalone, M.; Junge, K.; Beller, M. A biomass-derived non-noble cobalt catalyst for selective hydrodehalogenation of alkyl and (hetero)aryl halides. *Angew. Chem., Int. Ed.* **2017**, *56* (37), 11242−11247.

(51) Ramesh Naidu, B.; Venkateswarlu, K. WEPA: A reusable waste biomass-derived catalyst for external oxidant/metal-free quinoxaline synthesis via tandem condensation−cyclization−oxidation of α-hydroxy ketones. *Green Chem.* **2022**, *24* (16), 6215−6223.

(52) Ji, P.; Davies, C. C.; Gao, F.; Chen, J.; Meng, X.; Houk, K. N.; Chen, S.; Wang, W. Selective skeletal editing of polycyclic arenes using organophotoredox dearomative functionalization. *Nat. Commun.* **2022**, *13* (1), No. 4565.

(53) Charpe, V. P.; Ragupathi, A.; Sagadevan, A.; Hwang, K. C. Photoredox synthesis of functionalized quinazolines via copper-catalyzed aerobic oxidative Csp^2−H annulation of amidines with terminal alkynes. *Green Chem.* **2021**, *23* (14), 5024−5030.

(54) Barbosa da Silva, E.; Rocha, D. A.; Fortes, I. S.; Yang, W.; Monti, L.; Siqueira-Neto, J. L.; Caffrey, C. R.; McKerrow, J.; Andrade, S. F.; Ferreira, R. S. Structure-based optimization of quinazolines as cruzain and TbrCATL inhibitors. *J. Med. Chem.* **2021**, *64* (17), 13054−13071.

(55) Yu, C.; Guo, X.; Xi, Z.; Muzzio, M.; Yin, Z.; Shen, B.; Li, J.; Seto, C. T.; Sun, S. AgPd nanoparticles deposited on $WO_{2.72}$ nanorods as an efficient catalyst for one-pot conversion of nitrophenol/nitroacetophenone into benzoxazole/quinazoline. *J. Am. Chem. Soc.* **2017**, *139* (16), 5712−5715.

(56) Jin, H.; Li, P.; Cui, P.; Shi, J.; Zhou, W.; Yu, X.; Song, W.; Cao, C. Unprecedentedly high activity and selectivity for hydrogenation of nitroarenes with single atomic Co_1-N_3P_1 sites. *Nat. Commun.* **2022**, *13* (1), No. 723.

(57) Guo, X.; Hao, C.; Jin, G.; Zhu, H.-Y.; Guo, X.-Y. Copper nanoparticles on graphene support: An efficient photocatalyst for coupling of nitroaromatics in visible light. *Angew. Chem., Int. Ed.* **2014**, *53* (7), 1973−1977.

(58) Abu-Omar, M. M. High-valent iron and manganese complexes of corrole and porphyrin in atom transfer and dioxygen evolving catalysis. *Dalton Trans.* **2011**, *40* (14), 3435−3444.